Journal of Neuroscience Methods 309 (2018) 109–120

Contents lists available at ScienceDirect

Journal of Neuroscience Methods

journal homepage: www.elsevier.com/locate/jneumeth

Development and characterization of the InVesalius Navigator software for navigated transcranial magnetic stimulation

Victor Hugo Souza[a,*,1], Renan H. Matsuda[a], André S.C. Peres[a,b], Paulo Henrique J. Amorim[c], Thiago F. Moraes[c], Jorge Vicente L. Silva[c], Oswaldo Baffa[a]

[a] Departamento de Física, Faculdade de Filosofia, Ciências e Letras de Ribeirão Preto, Universidade de São Paulo, Av. Bandeirantes, 3900, 14040-901, Ribeirão Preto, SP, Brazil
[b] Instituto Internacional de Neurociência de Natal Edmond e Lily Safra, Instituto Santos Dumont, Rodovia RN 160 Km 03, 3003, 59280-000, Macaíba, RN, Brazil
[c] Núcleo de Tecnologias Tridimensionais, Centro de Tecnologia da Informação Renato Archer, Rodovia Dom Pedro I Km 143, 13069-901, Campinas, SP, Brazil

GRAPHICAL ABSTRACT

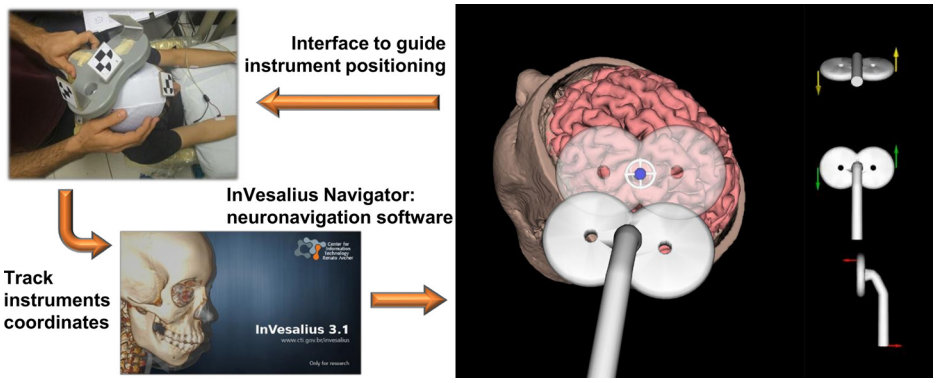

ARTICLE INFO

Keywords:
Neuronavigation
Transcranial magnetic stimulation
Localization error
Co-registration
Coil positioning
Surgical planning

ABSTRACT

Background: Neuronavigation provides visual guidance of an instrument during procedures of neurological interventions, and has been shown to be a valuable tool for accurately positioning transcranial magnetic stimulation (TMS) coils relative to an individual's anatomy. Despite the importance of neuronavigation, its high cost, low portability, and low availability of magnetic resonance imaging facilities limit its insertion in research and clinical environments.

New method: We have developed and validated the InVesalius Navigator as the first free, open-source software for image-guided navigated TMS, compatible with multiple tracking devices. A point-based, co-registration algorithm and a guiding interface were designed for tracking any instrument (e.g. TMS coils) relative to an

Abbreviations: AP, anterior-posterior; CT, computed tomography; FRE, fiducial registration error; InVNav–MTC, InVesalius Navigator with MicronTracker; InVNav–Patriot, InVesalius Navigator with Patriot; MRI, magnetic resonance imaging; FRE_{max}, maximum fiducial registration error; TRE_{max}, maximum target registration error; MTC, MicronTracker; NBS3.2–Spectra, NBS 3.2 with Spectra; NBS4.3–Vicra, NBS 4.3 with Vicra; StudyVar%, percentage of study variation; RL, right-left; SDK, software development kit; SI, superior-inferior; TRE, target registration error; TMS, transcranial magnetic stimulation; VTK, Visualization Toolkit

* Corresponding author at: Aalto University School of Science, Department of Neuroscience and Biomedical Engineering, P.O. Box 12200, FI-00076 AALTO, Finland.

E-mail addresses: victor.souza@aalto.fi (V.H. Souza), renan.matsuda@usp.br (R.H. Matsuda), peres@isd.org.br (A.S.C. Peres), paulo.amorim@cti.gov.br (P.H.J. Amorim), tfmoraes@cti.gov.br (T.F. Moraes), jorge.silva@cti.gov.br (J.V.L. Silva), baffa@usp.br (O. Baffa).

[1] Present address: Department of Neuroscience and Biomedical Engineering, Aalto University School of Science, P.O. Box 12200, FI-00076 AALTO, Finland.

https://doi.org/10.1016/j.jneumeth.2018.08.023
Received 16 June 2018; Received in revised form 7 August 2018; Accepted 20 August 2018
Available online 24 August 2018
0165-0270/

individual's anatomy.
Results: Localization, precision errors, and repeatability were measured for two tracking devices during navigation in a phantom and in a simulated TMS study. Errors were measured in two commercial navigated TMS systems for comparison. Localization error was about 1.5 mm, and repeatability was about 1 mm for translation and 1° for rotation angles, both within limits established in the literature.
Comparison with existing methods: Existing TMS neuronavigation software programs are not compatible with multiple tracking devices, and do not provide an easy to implement platform for custom tools. Moreover, commercial alternatives are expensive with limited portability.
Conclusions: InVesalius Navigator might contribute to improving spatial accuracy and the reliability of techniques for brain interventions by means of an intuitive graphical interface. Furthermore, the software can be easily integrated into existing neuroimaging tools, and customized for novel applications such as multi-locus and/or controllable-pulse TMS.

1. Introduction

Neuronavigation systems have been shown to be a valuable tool in clinical and research applications. A combination of spatial tracking devices and tomographic neuroimages such as computed tomography (CT) and magnetic resonance imaging (MRI) enables accurate, online localization of surgical and interventional instruments relative to the neuronal anatomy. An important application of neuronavigation is to provide accurate and stable positioning of the coil throughout a transcranial magnetic stimulation (TMS) session (Ruohonen and Karhu, 2010; Sollmann et al., 2016). Also, neuronavigation is commonly used to aid surgical planning (Grillo et al., 2018; Rondinoni et al., 2014), and to record the position of the brain scanner sensors, e.g., electroencephalography (Chiarelli et al., 2015), magnetoencephalography (Little et al., 2014) and optical diffusion spectroscopy (Tsuzuki and Dan, 2014), thereby allowing to combine functional information with anatomical brain images.

TMS is a non-invasive brain stimulation technique that has been used to study cortical brain function and to treat several neurological disorders (Rossini et al., 2015). The properties of the physiological responses elicited by TMS depend on the coil orientation and location (Ruohonen and Karhu, 2010; Souza et al., 2017). In this context, the use of navigation systems makes it easier to control the coil positioning within a defined displacement range and contributes to a reduction in response variability (Sollmann et al., 2016). Despite the well-accepted benefits of navigation systems, the high-cost, relatively low portability, and low availability of MRI facilities limit its insertion in research and clinical environments. Moreover, the majority of neuronavigation systems are closed platforms and are developed to work with only a single model of spatial tracking device in one operational system. Therefore, the development of low-cost, multiplatform and flexible alternatives is of utmost importance.

Recently, (Ambrosini et al., 2018) developed the StimTrack software for online TMS coil placement without the need of MRI. Moreover, several open-source projects have been developed aiming at image-guided navigation for surgical applications such as CustuX, SlicerIGT (Fedorov et al., 2012), MITK-ITC (Nolden et al., 2013) and NiftyIGI (Clarkson et al., 2015). However, none of these frameworks provides specific tools for image-guided coil placement in TMS.

Possible improvements in the flexibility of neuronavigation systems would be the ability to connect the navigation software with multiple spatial tracking devices. Spatial tracking devices record online translations and sensor rotations, which allows for monitoring the TMS coil and the subject's head positions. The sensor coordinates are recorded using optical, electromagnetic, or ultrasound transducers. Each of these devices has physical limitations; for instance, optical trackers require the space between the sensors and camera to be free from visual blocking. In turn, electromagnetic devices are affected by ferromagnetic parts in the near surroundings. Thus, case-specific application of a neuronavigation system in research or operatory environments might require a distinct spatial tracking device.

In order to overcome the limitations mentioned above for current neuronavigation systems, we have developed an extension of the InVesalius software program (Amorim et al., 2015) called the InVesalius Navigator. The extension allows communication with multiple tracking devices, tools for structural image processing and online TMS coil tracking, all combined in a user-friendly interface. InVesalius is a Python open-source, multiplatform, free software to analyze and visualize medical images. Also, InVesalius has an active worldwide community of contributors with users in over 144 countries. Moreover, Python has been used by many important packages and software tools in neuroscience, e.g., MNE (Gramfort, 2013), PsychoPy (Peirce, 2007), and MagPy (McNair, 2017), mainly for its ability to interface with different languages, easy syntax, high-level coding and a vast number of libraries. Altogether, these features make InVesalius a suitable platform to develop a free, open-source neuronavigation software.

This paper aims to validate and characterize the errors associated with the InVesalius Navigator software during a navigation procedure in a phantom and a simulated TMS study. Additionally, we compared the errors with two commercially available devices for navigated TMS.

2. Material and methods

2.1. Software development

InVesalius Navigator was developed in Python language combined with several freely available libraries such as wxPython for the graphical user interface, Visualization Toolkit (VTK) for visualization tools, Nibabel for neuroimaging support and Numpy for numerical data and array manipulation. A complete list of dependencies and download links are available on the InVesalius project website [https://www.cti.gov.br/invesalius].

Wrapping libraries were developed to enable access to the software development kit (SDK) of commercial spatial tracking devices. Communication to the following models was developed: MicronTracker (MTC) Sx60 (ClaroNav Inc., Toronto, Canada), Patriot, Fastrak and Isotrak II (Polhemus, Colchester, VT, USA). A combination of CMake (Kitware, Inc., Clifton Park, NY, USA), Swigwin (University of Utah, Salt Lake City, UT, USA) and Visual Community 2015 (Microsoft Corporation, Redmond, WA, USA) was used to generate and compile C++ libraries, and the source code of each SDK resulting in a portable Python package. Generated libraries and installation instructions are available with other dependency packages in the InVesalius repository on GitHub [https://github.com/invesalius/invesalius3]. All companies approved their distribution since no commercial source code is accessible within the wrapping libraries.

The pipeline to work with InVesalius Navigator was designed to provide an intuitive flow of the navigation procedure. In general, neuronavigation can be started in five steps. First, the user imports the subject's MRI or CT image set. In the case where no imaging facility is available, the user might alternatively import a brain template that contains an illustrative cortical morphology, such as the MNI152

(Fonov et al., 2011). Even though the accurate location of individual anatomic areas is not possible with a brain template, the navigator interface still controls the coil positioning within a defined target. Next, the user selects the volumetric reconstruction in ray casting or surface mode. InVesalius contains the watershed and region growing algorithms for the brain surface segmentation, and supports STL or OBJ files to import surfaces segmented with third-party tools. Both visualization modes provide the required anatomical insight of cerebral cortex to target the region of interest and fulfill the needs for navigated TMS.

In the third step, the user must select the desired spatial tracking device and register the desired instrument using the tracking probe. Then, they select three fiducials in the image and record the same three fiducial coordinates using the tracking device probe. Finally, the user must click on the Navigate button, and the navigation procedure will start. It is possible to create spherical markers for reference in 3D volume during the navigation. Markers can be created by clicking on the corresponding button, or by external trigger monitoring. The latter was developed for communicating with TMS devices and automatically creates the marker in positions where pulses were applied. Also, the user can define a marker as a target, and enable an interface to guide the instrument positioning within a user-defined range of acceptance in translation and rotation angles. The target interface enables multi-session reliability of positioning instruments in several applications such as navigated TMS. The software runs on personal computers and laptops with at least 4 GB of RAM, multi-core processors with 2.0 GHz and 300 MB of hard-disk drive free space for installation. Graphics cards are not mandatory, but may significantly increase 3D rendering quality and speed. InVesalius also can take advantage of GPU processing to optimize rendering.

2.2. Co-registration method

The co-registration algorithm is a set of matrix multiplications that transforms coordinates provided by the tracking device (i.e. the physical space) to the user interface in the software (i.e. virtual space). Overall, the co-registration algorithm comprises creation of two reference frames with the tracking device probe (i.e. instrument and head) and one reference frame for the head's image within the software. Thus, the tracking sensor coordinates attached to the instrument are transformed to the instrument's reference frame, then transformed to the head's reference system, and finally to the head's image frame in the software. The transformations are described below step-by-step. Three tracking sensors are used during the procedure: a probe to record the fiducial points, a reference sensor attached to a rigid part of the head, and a third sensor attached to an instrument (e.g. a TMS coil). Hereafter, we adopted the notation in which a matrix ${}^{inst}_{base}M_{trk}$ represents a change of basis matrix ${}_{base}M$ composed by a translation T followed by a rotation R, from the tracking device reference system (trk) to the instrument reference system (inst). No shearing or scaling is used.

First, a translation is applied from the fixed position of the sensor in the instrument to the desired point of interest (e.g. the center of the coil) to create the reference frame of the instrument. Then, the reference frame of the coil is created by collecting three fiducials distributed around the point of interest in the tracking device reference frame and computing a change of basis matrix ${}^{inst}_{base}M_{trk}$, using a custom-made method described in Appendix A. During this step, the instrument must be fixed with the third sensor attached to it. The initial position and orientation of the attached sensor given in the tracker reference frame is ${}^{inst}M_{0trk}$, a composition of a rotation ${}^{inst}R_{0trk}$ and a translation ${}^{inst}T_{0trk}$. The transformation to the point of interest is then applied in every iteration during the navigation using the following equation:

$$ {}^{inst}M_{trk} = {}^{probe}R_{trk}({}^{probe}M_{0trk})^{-1}({}^{probe}R_{0trk})^{-1}{}^{probe}R_{trk}\,{}^{inst}_{base}M_{trk}\,{}^{probe}M_{0trk}\,{}^{probe}T_{trk} \quad (1) $$

where ${}^{probe}R_{trk}$ and ${}^{probe}T_{trk}$ are the instantaneous probe rotation and translation in the tracking reference frame. Next, the coordinate of the instrument is transformed to the reference sensor attached to the head to correct for possible movements by the subject.

$$ {}^{inst}M_{ref} = {}^{ref}M_{trk}^{-1}\,{}^{inst}M_{trk} \quad (2) $$

where ${}^{inst}M_{ref}$ is the instrument transformation matrix given in the head reference sensor frame. Then, we apply the change from physical to virtual space using ${}^{img}M_{ref}$ in two separate steps for rotation and translation. ${}^{img}M_{ref}$ is computed using the quaternion-based algorithm by Horn, 1987, and the three fiducials collected in the nasion, left and right tragus with coordinates given in both virtual space and tracker reference space. Construction of the head's reference frame is independent from the instrument's reference frame and might be performed in any order before the navigation starts. Next, the translation and rotation from instrument to image space are given by:

$$ {}^{inst}T_{img} = {}^{img}M_{ref}\,{}^{inst}M_{ref} \quad (3) $$

$$ {}^{inst}R_{img} = {}^{inst}_{base}R_{img}({}^{inst}_{base}M_{trk})^{-1}({}^{inst}M_{0ref})^{-1}{}^{inst}M_{ref}\,{}^{inst}_{base}M_{trk} \quad (4) $$

where ${}^{inst}_{base}R_{img}$ is the rotation component of a change of basis matrix computed with the method shown in Appendix A, and the instrument fiducials are given in the virtual space. Finally, the affine matrix is composed using the translation represented in homogeneous coordinates by ${}^{inst}T_{img}$, and the (3×3) rotation matrix component in ${}^{inst}R_{img}$. The result is the transformation matrix ${}^{inst}M_{img}$ that is directly applied to the object representing the instrument in the visualization scene of the software.

2.3. Characterization of co-registration method

2.3.1. Phantom design

A cubic acrylic phantom with 21.10 ± 0.05 cm length was manufactured with dimensions comparable to the average human head for characterizing the navigation systems (Fig. 1 A). The 3D axes were named anterior-posterior (AP), right-left (RL) and superior-inferior (SI) for correspondence with conventional medical imaging orientation systems. Nylon wires with 0.25 ± 0.05 mm diameter were interlaced inside the acrylic cube composing an inner cube with an edge length of 100.00 ± 0.05 mm, and 1331 intersecting points. Every crossing point in the inner cube was distant from its first neighbors by 10.00 ± 0.05 mm in all axes.

Virtual simulated tomographic images of the cubic phantom were produced using a MATLAB 2015a (MathWorks Inc., Natick, MT, USA) script to mimic a conventional 3D T1-weighted structural MRI acquired with a gradient echo sequence, repetition time of 6.7 ms, echo time of 3.1 ms and $(256 \times 265 \times 180)$ acquisition matrix with pixel size of $(1 \times 1 \times 1)$ mm^3. Each crossing point in the acrylic phantom was represented by a voxel value of 255, shown in Fig. 1B, resulting in a framed virtual cube with an edge length of 100 mm, and identical to the measurement volume of the acrylic phantom.

2.3.2. Experimental procedure

The experiment was performed in distinct sessions using InVesalius Navigator connected to MTC (InVNav–MTC) and Patriot (InVNav–Patriot). InVesalius Navigator was installed in a personal computer with Windows 10, CPU Intel i7 2.8 GHz, 8 GB RAM and a NVidia GeForce GT 640 graphics card. The same measurements were also performed with the navigated TMS software NBS 3.2, and NBS 4.3 (Nexstim Plc, Helsinki, Finland) connected to the Polaris Spectra (NBS3.2–Spectra) and Vicra (NBS4.3–Vicra) (Northern Digital Inc., Waterloo, ON, Canada) optical tracking systems, respectively, for comparison with commercially available systems.

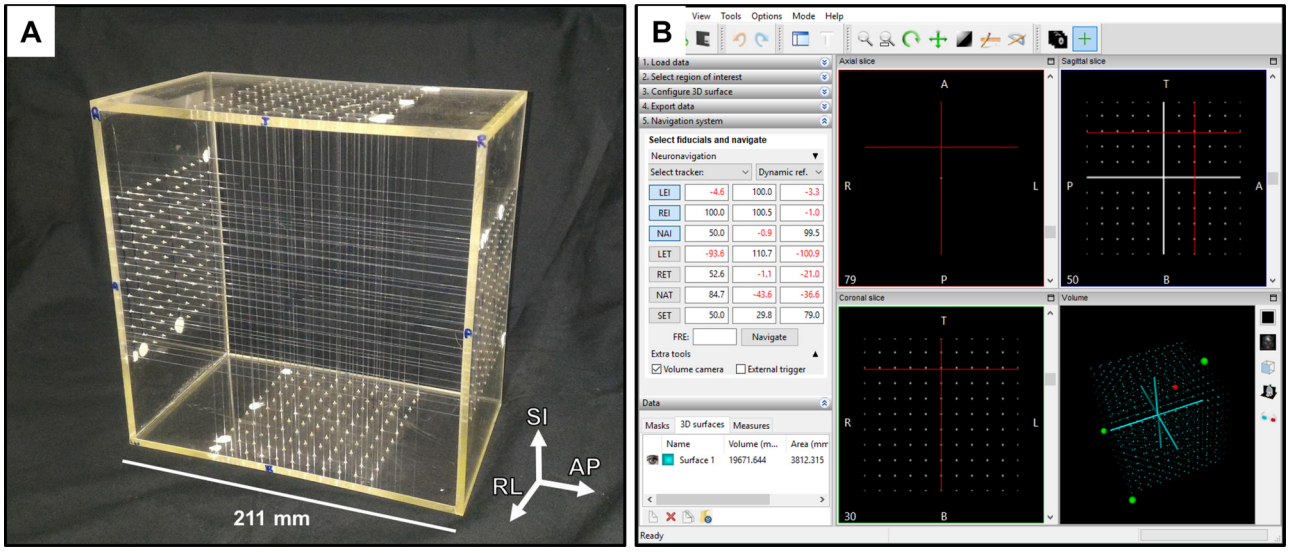

Fig. 1. (A) Picture of the acrylic phantom. The coordinate system indicates the anterior-posterior (AP), right-left (RL) and superior-inferior (SI) axes. (B) Screenshot of InVesalius Navigator with phantom image slices in coronal, sagittal and axial views, and 3D visualization of points representing the crossing wires used for system characterization. Green markers represent the fiducials used for co-registration and the red marker is the real-time location of the tracking device probe. (For interpretation of the references to colour in this figure legend, the reader is referred to the web version of this article.)

Phantom images were imported to the corresponding navigation software and split in axial, sagittal, and coronal views. Next, a volumetric reconstruction of all measurement points was created using the InVesalius tools to obtain 1.0 mm diameter spheres in the volumetric rendering space, shown in Fig. 1B. For co-registration, fiducials were selected to resemble the locations of nasion, left and right tragus commonly used in human applications. Selected fiducials were right and left extremities of the intersection line between the posterior and inferior planes, and the midpoint of the intersection line between the anterior and superior planes. Coordinates were recorded using the digitization function available in InVesalius Navigator and NBS.

Measurements were performed manually placing the tracking probe tip and digitizing the coordinates of each crossing point in four planes along the RL axis. Points were located every 10.00 ± 0.05 mm within each plane along the AP and SI axis. Plane 1 was next to the cube's left face. Distances between planes number 2, 3 and 4 to plane 1 were: 10.00 ± 0.05 mm, 50.00 ± 0.05 mm and 100.00 ± 0.05 mm, respectively. The inner cube had an edge length of 100.00 ± 0.05 mm, composing the measurement volume. The measurement sequence started from the point in the upper anterior corner of the phantom. The experiment was performed within the operational range provided by the manufacturers of all tracking devices: 152 cm for Patriot, 115 cm for MTC, 134 cm for Vicra and 240 cm for Spectra. The entire procedure was repeated three times for each device.

2.3.3. Data analysis

Analysis consisted in computing the error related solely to the developed co-registration algorithm with the fiducial registration error (FRE). Next, the error of targeting each point in space, represented by a pair of crossing lines in the phantom, was estimated for the given fiducial configuration using the target registration error (TRE). FRE was computed as the root mean square distance from the fiducial coordinates to its counterpart after the co-registration (Fitzpatrick et al., 1998), given by:

$$FRE^2 \equiv \frac{1}{n}\sum_{i=1}^{n} |(Q_E + (M^{-1}.N)(P_{Hi} - Q_H)) - P_i|^2 \quad (5)$$

where P_i is the image fiducial i, P_{Hi} is the correspondent fiducial in the tracker reference frame, M is the change of basis from the image reference frame to the basis created using the fiducials in image space, N is the change of basis from the tracker reference frame to the basis of fiducials in the tracker space, n is the total number of fiducials, and Q_E and Q_H are the origins of image and tracker reference frames, respectively. In turn, TRE represents the distance between a target point other than fiducials and its counterpart after co-registration. TRE was estimated as proposed by Fitzpatrick et al. (1998):

$$\langle TRE^2(r)\rangle \approx \frac{\langle FRE^2\rangle}{(n-2)}\left(1+\frac{1}{3}\sum_{k=1}^{3}\frac{d_k^2}{f_k^2}\right) \quad (6)$$

where the given fiducials configuration results in a principal axis k, f_k is the root mean square distance between the fiducials to the principal axis and d_k is the distance between the target to the principal axis. TRE was estimated using the maximum FRE obtained among all characterization runs for a given device.

Lastly, system accuracy and precision during the navigation procedure were measured. The accuracy was named as localization error and computed as the Euclidian distance between the coordinates recorded in image space during navigation and the actual coordinates in the simulated phantom image. Average localization error was estimated across all 484 points for each navigation system. Precision was estimated as the standard deviation of the average localization error (Kuehn et al., 2008).

One-way analysis of variance (ANOVA) was applied to investigate how localization error differed between navigation systems; residual plots did not reveal any apparent deviations from normality. Tukey HSD was used for post hoc multiple comparisons. Statistical analysis was performed in R 3.4 (R Core Team, Vienna, Austria) and the level of significance was set at 5%.

2.4. Validation of instrument position and orientation control

The experimental validation of instrument positioning and control during neuronavigation was employed in InVNav–MTC and InVNav–Patriot systems. A dummy head and a TMS figure-eight coil (Neurosoft, Ivanovo, Russia) were used to compute the repeatability of estimating the rotation angles and translation vector during navigation in an experiment based on the study by Ambrosini et al. (2018). The dummy head was filled with a solution composed of 3.6 g of NaCl and 1.95 g of $CuSO_4{\cdot}5H_2O$ per liter of H_2O (Peres et al., 2009). An MRI of the dummy head was acquired in a Achieva 3 T scanner (Philips Healthcare, Best, The Netherlands) with a gradient echo sequence,

acquisition matrix of (256 × 256 × 156), FOV of 256 mm, and a voxel size of (1 × 1 × 1) mm. The MRI was imported to InVesalius Navigator for co-registration using nasion, right and left tragus fiducials. The dummy head was attached to a table, and the coil was held by a mechanical arm. The center of the coil was placed over the area representing the primary motor cortex. Measurements of the transformation matrix were performed in three experimental conditions for two different targets in each hemisphere, left and right. Three conditions

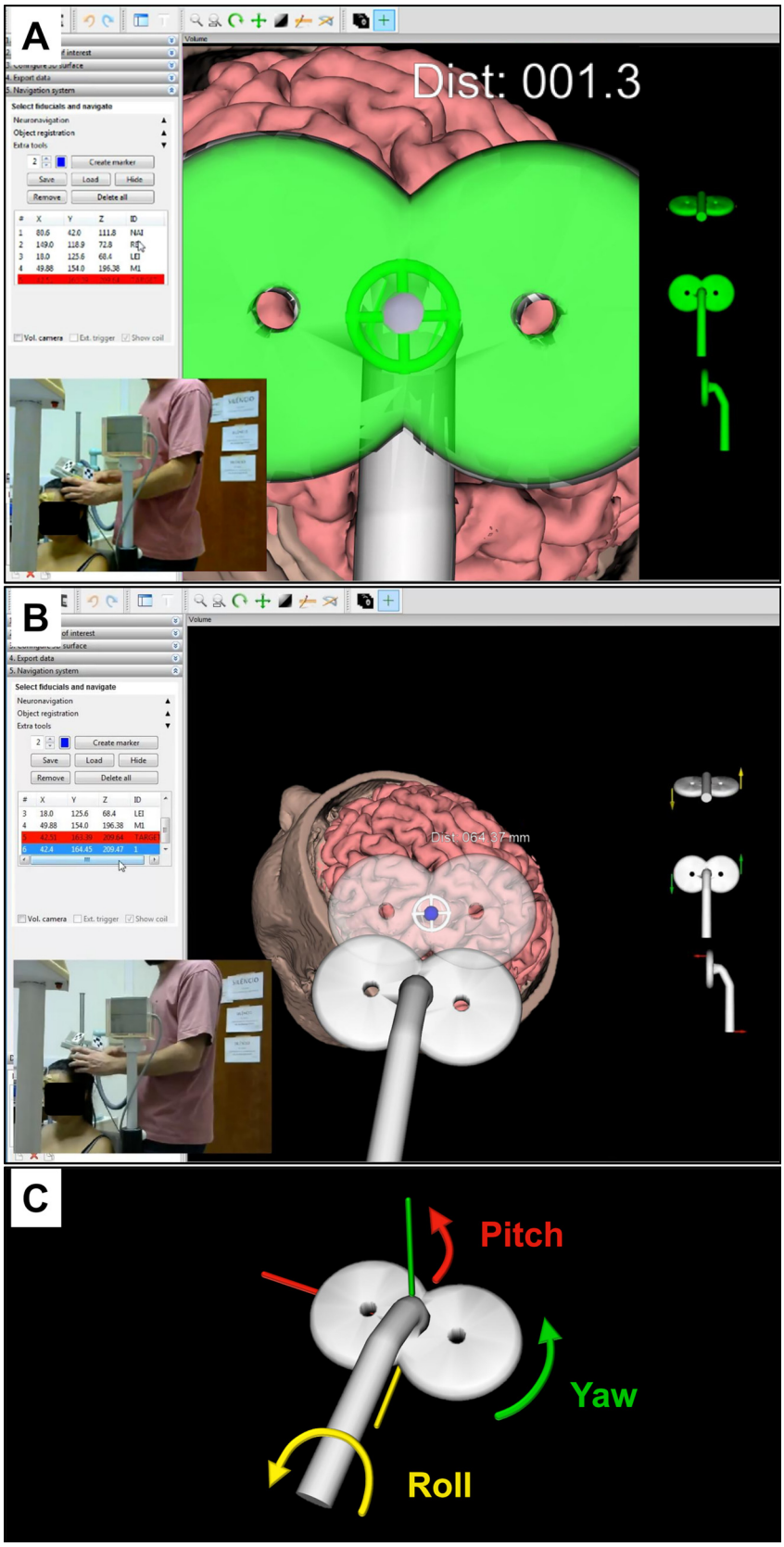

Fig. 2. InVesalius Navigator interface used for positioning a TMS coil relative to a defined target (A) with all coil coordinates adjusted within acceptance limits predefined by the user, and (B) with coil shifted and rotated away from the desired position. The white number above the TMS coil and preceded by the term "Dist" indicates the distance to the target. The angular differences are represented by updating the yellow, green and red arrow length shown in the right lateral panel containing three small TMS coils in (B). Each small coil turns green if the difference in coordinate is lower than the user-defined limits, as shown in the right lateral panel of (A). (C) Schematic representation of the rotation angles used for characterization and validation of InVesalius Navigator. The term yaw represents the coil bearing, the pitch stands for the elevation and roll for the bank angle. (For interpretation of the references to colour in this figure legend, the reader is referred to the web version of this article.)

were used for each target. Condition 1 corresponded to the head sensor in position one and coil registration one; condition 2 corresponded to the head sensor in position two and coil registration one; and condition 3 represented the head sensor in position two and coil registration two. Head sensor position one and two were left and right sides of the forehead, respectively. Coil registration one and two for Patriot corresponded to the tracker sensor placed on the face and handle of the coil, respectively. For MTC, the coil sensor was placed on the left and right edges on the coil face, respectively for registration one and two. Co-registration was repeated ten times, and the translation vector and rotation angles were extracted from the transformation matrix in each trial. An additional run was performed with the head sensor in position two and coil registration one to evaluate the static fluctuations of coordinates during navigation. In this case, coordinates were sampled every 2 s for 180 s, with coil and head static during navigation.

Repeatability was estimated for the translation vector (i.e. Euclidian distance) and angle difference to the target using the Gage R & R measurement system assessment in the SixSigma R 3.4.0 software package (R Core Team).

2.5. Localization error for revisiting a target

InVesalius Navigator localization error associated with repositioning the stimulation coil multiple times relative to a defined target was estimated in a simulated TMS experiment. The experiment was performed for InVNav–MTC and InVNav–Patriot systems. Three adults (two men and one woman, 24, 26 and 29 years old) with non-reported neurological or motor diseases participated in this study. All subjects were submitted to a volumetric gradient echo T1-weighted MRI in a Achieva 3 T scanner (Philips Healthcare) with (240 × 240 × 240) acquisition matrix and a voxel size of (1 × 1 × 1) mm. The study was approved by the local ethics committee of the University of São Paulo (CAAE: 54674416.9.0000.5407) in accordance with the Declaration of Helsinki, and each participant gave written informed consent before the experiment.

Participants sat comfortably in a reclining chair and were asked to stay fully relaxed, following the same procedures as in a conventional TMS experiment (Julkunen, 2014). The MRI was imported to InVesalius Navigator, a volumetric rendering was constructed, and co-registration performed using the nasion, left and right tragus fiducials. The hand knob identified in the left primary motor cortex of the subject's MRI is commonly used in TMS experiments (Sollmann et al., 2016), and was marked as a target. A TMS figure-eight coil was positioned approximately tangential to the scalp, directly above the target, and the coordinates were saved in InVesalius Navigator. The coil was initially placed on a table by the left side of the subject. The coil was moved from the initial position to the target following the InVesalius Navigator guiding interface, shown in Fig. 2. When the user was able to hold the coil steady within the range of 3 mm for distance and 3° for each rotation angle, a marker was created simulating a TMS pulse, and the coil moved back to the initial position. This procedure was repeated ten times for three head co-registrations.

Localization error related to revisiting a target was computed as the average Euclidian distance, and angle deviations in each axis between every marked spot and the selected target. Two-way ANOVA was used to assess if differences in coordinates varied for each tracking device (InVNav–MTC and InVNav–Patriot) and coordinate (translation, yaw, pitch, and roll). Fig. 2C shows the yaw (coil bearing), pitch (coil elevation) and roll (coil bank angle) rotation angles relative to the TMS coil reference frame. Post hoc multiple comparisons were performed using Tukey HSD test, and the level of significance was set at 5%.

3. Results

3.1. Software validation

The FRE, TRE, mean localization and precision errors for InVNav–MTC and InVNav–Patriot, and NBS3.2–Spectra and NBS4.3–Vicra systems are depicted in Table 1. Figs. 3 and 4 illustrates the spatial distribution of TRE, and localization error for all tested systems, respectively. Every marker coordinate corresponds to a pair of crossing lines measured in the acrylic phantom, and the color scale shows the computed quantity (i.e. TRE or localization error).

Localization error representing the distance between measured and targeted coordinates varied across the navigation systems, revealing a slightly lower error for NBS systems compared to InVNav–MTC and InVNav–Patriot ($F_{3,1932} = 70.48$; $p < 0.001$). Post hoc multiple comparisons indicated that mean localization error for NBS3.2–Spectra significantly deviated 0.34 and 0.40 mm from InVNav–MTC and InVNav–Patriot, respectively. Additionally, NBS4.3–Vicra was significantly different from InVNav–MTC and InVNav–Patriot at 0.29 and 0.35 mm, respectively. No relevant differences were identified between InVNav–MTC and InVNav–Patriot, and no difference between NBS3.2–Spectra and NBS4.3–Vicra. A boxplot of localization errors for each system is depicted in Fig. 5.

3.2. Validation of instrument position and orientation control

The repeatability and study variation percentage (StudyVar%) resulting from the Gage R & R study are described in Table 2 for InVNav–MTC and InVNav–Patriot. The measurements in the Gage R & R study are accurate if the contribution of the gage variability to the total study variability (i.e. StudyVar%) is lower than 10%. The system is considered acceptable if the StudyVar% is between 10 and 30%. The system is not accurate for values greater than 30% due to large variations across measurements.

Fig. 6 illustrates the distance to the target in translation vector and rotation angles recorded for 180 s with the TMS coil and fixed dummy head. The largest deviations were obtained for translation with an upper limit of 1.52 mm, and yaw with an upper limit of 1.29°, both for InVNav–MTC. All values were within the range of ± 2 mm and ± 2° for InVNav–MTC, while all values were within + 0.3 and – 0.05 mm and degrees for InVNav–Patriot.

Table 1
Maximum FRE (FRE_{max}) and maximum TRE (TRE_{max}), average and 95th percentile of localization error and average precision error for InVesalius connected to MTC and Patriot (InVNav–MTC and InVNav–Patriot, respectively), Nexstim NBS 3.2 connected to Spectra (NBS3.2–Spectra), and Nexstim NBS 4.3 connected to Vicra (NBS 4.3–Vicra).

Navigation system	FRE_{max} (mm)	TRE_{max} (mm)	Localization error (mm)	Percentile 95th (mm)	Precision (mm)
InVNav–MTC	0.38	1.02	1.46	2.41	0.52
InVNav–Patriot	0.40	1.08	1.52	2.55	0.58
NBS3.2–Spectra	0.25	0.67	1.12	2.11	0.46
NBS4.3–Vicra	0.72	1.94	1.17	2.29	0.56

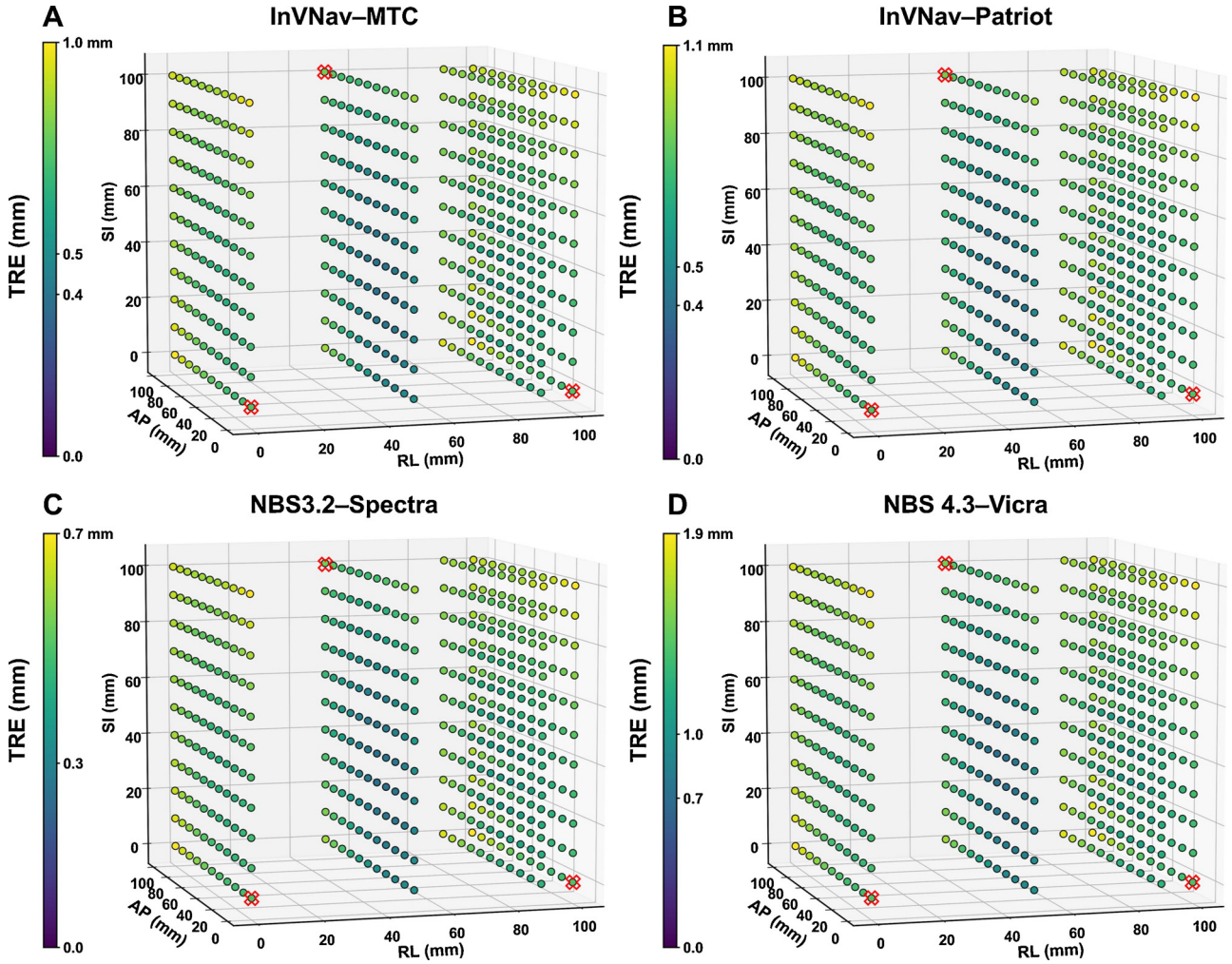

Fig. 3. Target registration error (TRE) distribution estimated for the cubic phantom used for characterization of (A) InVesalius connected to MTC (InVNav–MTC), (B) InVesalius connected to Patriot (InVNav–Patriot), (C) Nexstim NBS 3.2 connected to Spectra (NBS3.2–Spectra), and (D) Nexstim NBS 4.3 connected to Vicra (NBS4.3–Vicra). Red markers represent the location of fiducial points, and the four planes are located along the right-left (RL) axis of the acrylic phantom. TRE for each point is represented by the color scale. (For interpretation of the references to colour in this figure legend, the reader is referred to the web version of this article.)

3.3. Localization error for revisiting a target

In the TMS experiment, difference to target varied between the coordinates of interest ($F_{3,952} = 210.76$; $p < 0.001$) and for the interaction effect of coordinate and tracking device ($F_{3,952} = 6.24$; $p < 0.001$). However, no significant effect of tracking device on the difference of measurements to target was found ($F_{1,952} = 2.84$; $p = 0.092$). Post hoc multiple comparisons revealed a significant variation of 0.44° in pitch between InVNav–Patriot and InVNav–MTC ($p = 0.005$). Fig. 7 illustrates the comparison of all assessed coordinates between the two tracking devices connected to InVesalius Navigator.

4. Discussion

Herein we have described the development of an open-source neuronavigation software compatible with multiple tracking devices and with specific tools for TMS experiments. Our results indicate that registration and localization errors associated with the developed co-registration algorithm were low enough to provide good target localization and repeatability across multiple sessions. The overall localization and precision errors of the developed system are comparable to commercially available systems measured with a phantom and in a simulated TMS experiment.

4.1. InVesalius Navigator and NBS characterization

InVesalius Navigator and NBS systems showed an FRE below 1 mm for all runs of measurements. The obtained values are in the range of those reported in the literature for several navigation systems (Kuehn et al., 2008; Omara et al., 2014; Ruohonen and Karhu, 2010; Sollmann et al., 2016). Even though the FRE is primarily used to indicate the accuracy of the navigation procedure, its interpretation is limited to the quality of the registration procedure and fiducial points (Fitzpatrick et al., 1998). Therefore, maintaining a low FRE may prevent error propagation throughout the navigation procedure. The obtained FRE for InVesalius Navigator below 0.5 mm suggests that the proposed three-point fiducial co-registration algorithm is suitable for neuronavigation.

The TRE was estimated for all crossing points of the phantom considering each navigation system's maximum FRE in order to assess the specific error to locate a target point in space. Maximum estimated TRE was about 1 mm for all tested devices, except for NBS4.3–Vicra at about 1.9 mm. The highest TRE for NBS4.3–Vicra is probably due to the substantial maximum FRE compared to other systems, as the TRE computed by Eq. (6) is directly proportional to the FRE. This observation highlights the importance of carefully selecting fiducials, as larger registration errors may enhance the accuracy to locate a point in space.

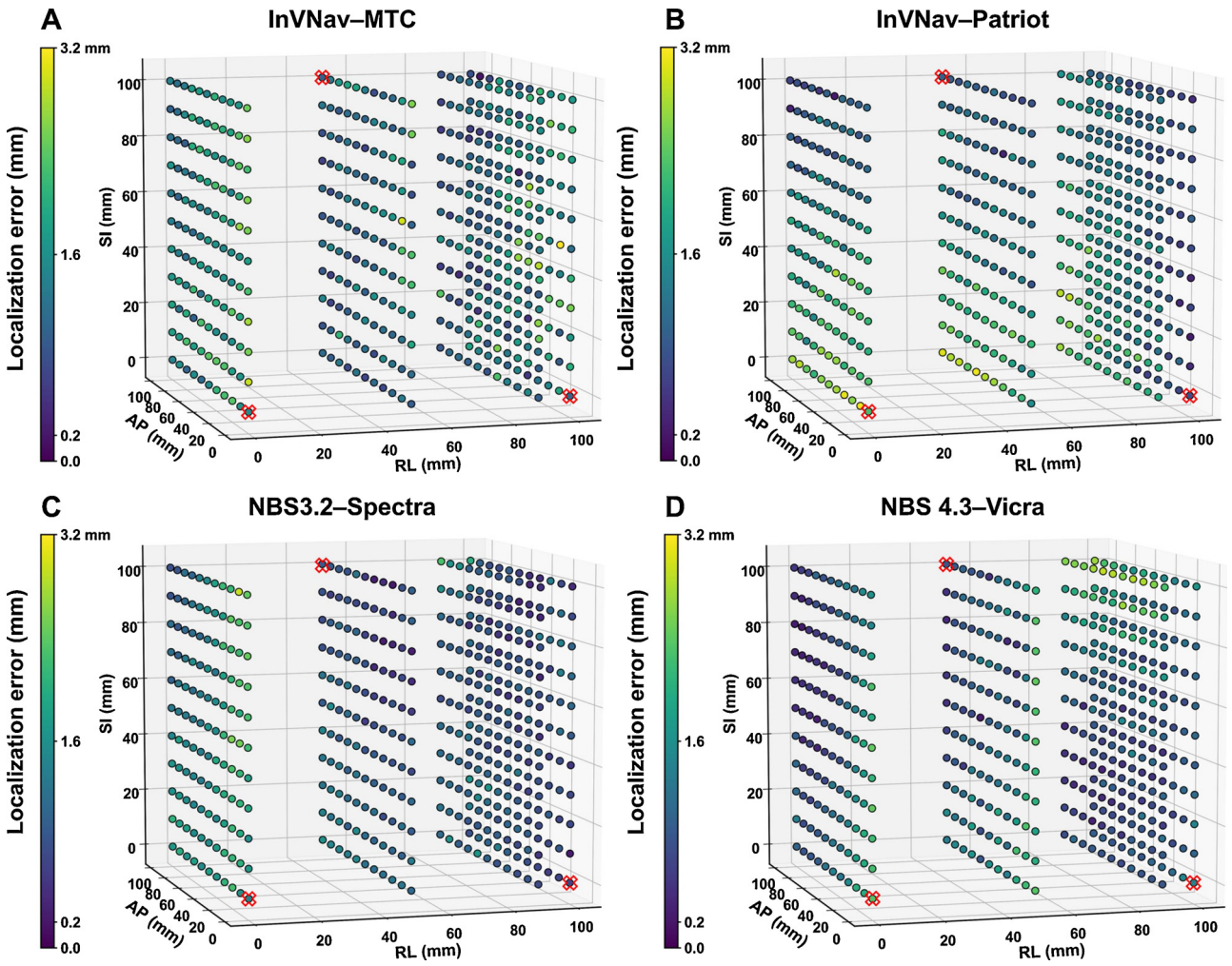

Fig. 4. Localization error distribution measured for (A) InVesalius connected to MTC (InVNav–MTC), (B) InVesalius connected to Patriot (InVNav–Patriot), (C) Nexstim NBS 3.2 connected to Spectra (NBS3.2–Spectra), and (D) Nexstim NBS 4.3 connected to Vicra (NBS4.3–Vicra). Marker coordinates correspond to the crossing wires in the acrylic phantom assessed with the tracking device probe during neuronavigation. Red markers represent the location of fiducial points and color scale represents the localization error. (For interpretation of the references to colour in this figure legend, the reader is referred to the web version of this article.)

Fig. 3 illustrates the spatial distribution of TRE for all points measured in the phantom. Points close to the centroid of the fiducials' configuration showed the lowest TRE, while points with highest TRE were located opposite to the plane containing the fiducials. This observation corroborates the theory of TRE proposed by Fitzpatrick et al. (1998), pointing out that the region of lowest TRE is close to the principal axis of the point set used for co-registration. Even though the TRE may be reduced for co-registration algorithms with a higher number of fiducial markers, the estimated location errors seem to be low enough to provide accurate navigation.

The localization and precision errors obtained for all tested navigation systems are lower than the recommended limits for frameless systems, 2–3 mm for mean localization error (Orringer et al., 2012; Steinmeier et al., 2000) and 3–4 mm for the 95th percentile (Mascott, 2006; Poggi et al., 2003), and lower than frame-based systems with 95th percentile of 3–5 mm (Maciunas et al., 1992). Moreover, NBS systems showed lower localization error of about 0.4 mm compared to InVesalius Navigator. The higher resolution and lower measurement fluctuations observed on the NBS3.2–Spectra and NBS4.3–Vicra tracking devices compared to InVNav–MTC and InVNav–Patriot probably explain the lower error for NBS systems. However, this deviation in the main applications of interest for InVesalius Navigator might be negligible, as the mean localization error for all systems were about 1.5 mm; half of the maximum recommended in the literature (Ruohonen and Karhu, 2010; Steinmeier et al., 2000).

Localization error spatial distribution showed lower values around the top part of the phantom, and higher error on the bottom-most region, as shown in Fig. 4. Possible explanations for the localization error inhomogeneous spatial variation are the spatial inhomogeneity in co-registration error and difficulty in accessing the points in the phantom. The target error given by the co-registration algorithm depends on the distance from the fiducial points' centroid (Fitzpatrick et al., 1998). The region around the centroid showed the lowest TRE, while the most distant corners resulted in the highest errors, thus affecting the localization error depending on the spatial location of each point. In addition, accessing all the points in the phantom required different probe entry maneuvers. Central, anterior and posterior areas were easily accessible, while the top and bottom points were accessed with increased difficulty, mainly because it required the probe to pass through the entire network of crossing nylon lines. This issue possibly led to an increase in the obtained localization error.

The main factors influencing the neuronavigation accuracy are co-registration method, tracking devices technical specifications, image parameters, and clinical events such as brain shift (Steinmeier et al., 2000). The phantom built for this study enabled assessment of the first two factors, and our results indicate that errors associated to our system are comparable to those of commercially available devices (Kuehn et al., 2008). Geometric imaging distortions might be disregarded in our

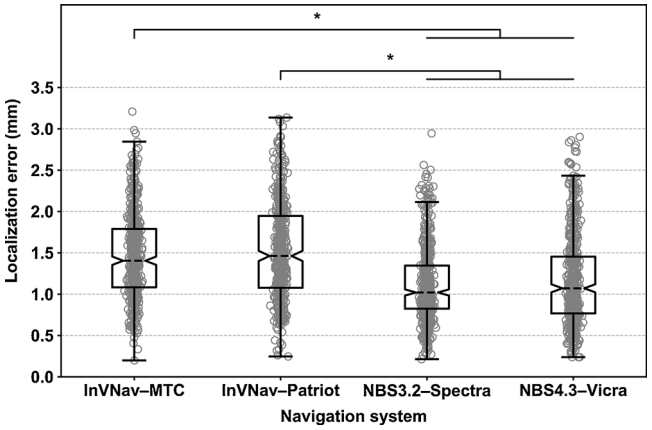

Fig. 5. Measurements of localization error on InVesalius connected to MTC and Patriot (InVNav–MTC and InVNav–Patriot, respectively), Nexstim NBS 3.2 connected to Spectra (NBS3.2–Spectra), and Nexstim NBS 4.3 connected to Vicra (NBS 4.3–Vicra). The box in the boxplot extends from the first to the third quartile of the data with the horizontal dashed line as the median, the notch represents the confidence interval around the median and the whiskers extend to the first data point equal to or 1.5 times less beyond the interquartile range. The gray circles represent the Euclidian distance between each measured coordinate in image space during navigation, and the actual coordinate in the simulated phantom image. * $p < 0.05$.

study because the phantom tomographic image was created using a computational algorithm. Moreover, MRI distortions have already been shown to have a low effect on the navigation accuracy (Steinmeier et al., 2000). Also, clinical events that may arise from the brain and positional shifts during the procedure may also have minimal impact on non-invasive applications such as a TMS experiment.

It should be noticed that the position of the phantom points may vary due to the nylon wires' flexibility. Therefore, it possibly overestimates the navigation system's error if compared to other rigid phantoms. However, the flexible material was employed to allow the probe insertion through the phantom, and to access the internal points. Moreover, the dimensions approximating a human head provided an overall visualization of spatial distribution errors relative to the fiducial markers. Considering that localization error is unevenly distributed in space, the development of a phantom with realistic head geometry would be a critical improvement to provide an assessment of errors with anatomical references.

4.2. InVesalius Navigator accuracy for revisiting a target

MTC and Patriot devices connected to InVesalius provided stable measurements of position and orientation during a 3-minute recording, as shown in Fig. 6. Translation and angular coordinates were critically lower than the acceptance range of 3 mm or 3°. Fluctuations of measurements with InVNav–Patriot were lower than 0.2 mm in translation, and within 0.05° in every orientation. Interestingly, InVNav–MTC showed larger variations than InVNav–Patriot, with higher range limits in translation and yaw angle of about 1.5 mm and 1.3°, respectively. The larger variations in translation compared to other coordinates is possibly explained by the fact that it sums x, y and z coordinates, and thus might be more sensitive to fluctuations in measurements from tracking devices. Overall, the apparent reduced stability of MTC compared to Patriot might be due to a more complex set of factors influencing the visible light camera-based algorithm compared to the electromagnetic measurement given by Patriot. Also, optical markers attached to the TMS coil in this experiment were relatively small compared to the camera-sensor distance during navigation. The stability of measurements with MTC can possibly be improved by designing suitable, larger optical markers for better acquisition of coordinates with the camera.

Assessment of the TMS coil position and orientation across distinct registrations revealed a repeatability level below 1 mm or 1° in all coordinates for InVNav–MTC and InVNav–Patriot. The obtained repeatability is critically lower than the values recommended in the literature (Ruohonen and Karhu, 2010; Sollmann et al., 2016). The Gage R & R study showed high variability in pitch and roll angles for both systems compared to translation and yaw. Both angles are partially aligned with the force direction applied by the handle to support the coil's weight. Thus, a greater variation might be expected in elevation and roll orientations, in which the balance of forces is more critical. Nevertheless, the repeatability and variation were lower than the tolerance for neuronavigation (i.e. 3 mm) and might not significantly affect the navigation accuracy. Therefore, the registration algorithm of InVesalius Navigator provides accurate measurements of coil position and orientation within multiple combinations of head and instrument registrations.

Finally, the target revisiting experiment for InVNav–MTC and InVNav–Patriot systems enabled instrument placement within a distance to the target of 3 mm or 3°. Interestingly, the difference in pitch angle varied between InVNav–MTC and InVNav–Patriot. Ambrosini et al. (2018) also reported a difference in positioning of pitch angle between StimTrack and BrainSight (Rogue Research Inc., Montreal Canada). Considering that pitch is the elevation angle that moves the tracking sensor attached to the coil farther away from the plane of the camera, there might be a decrease in measurement agreement in this specific coordinate. In turn, Patriot seems to be less affected in this specific orientation and might provide a better estimate. In summary, the guiding interface for the TMS coil positioning provided an accurate return to the target across the different instrument and head co-registrations.

Regarding TMS applications, it is important to note that the current navigation algorithm of InVesalius Navigator does not project the stimulation target to the brain cortical surface, as in line-navigated and electric-field-navigated commercial software. Both methods of navigated TMS have been shown to locate the stimulation targets distant from about 10 mm, which may lead to different motor mapping representations in presurgical applications (Sollmann et al., 2016). InVesalius Navigator allows the operator to use the TMS coil location and orientation relative to the MRI for offline processing of stimulation target and computation of electric field. In the future, online electric field computation should be incorporated to the InVesalius Navigator pipeline, which might enable better target localization with a lower number of pulses, and respecting each subject's anatomy (Laakso et al., 2018). Furthermore, one should note that even though no physiological measurements were performed in this study, the obtained repeatability and localization error ensure reliable TMS coil positioning throughout multiple sessions.

Table 2
Repeatability as standard deviations and the total study variation percentage (StudyVar%) estimated from the Gage R & R study on InVesalius connected to MTC and Patriot (InVNav–MTC and InVNav–Patriot, respectively).

System Repeatability	Translation (mm)/StudyVar%	Yaw (°)/StudyVar%	Pitch (°)/StudyVar%	Roll (°)/StudyVar%
InvNav–MTC	0.95/9.65%	0.86/2.81%	0.91/13.66%	0.80/9.70%
InVNav–Patriot	0.64/7.55%	0.50/2.64%	0.52/22.49%	0.58/18.15%

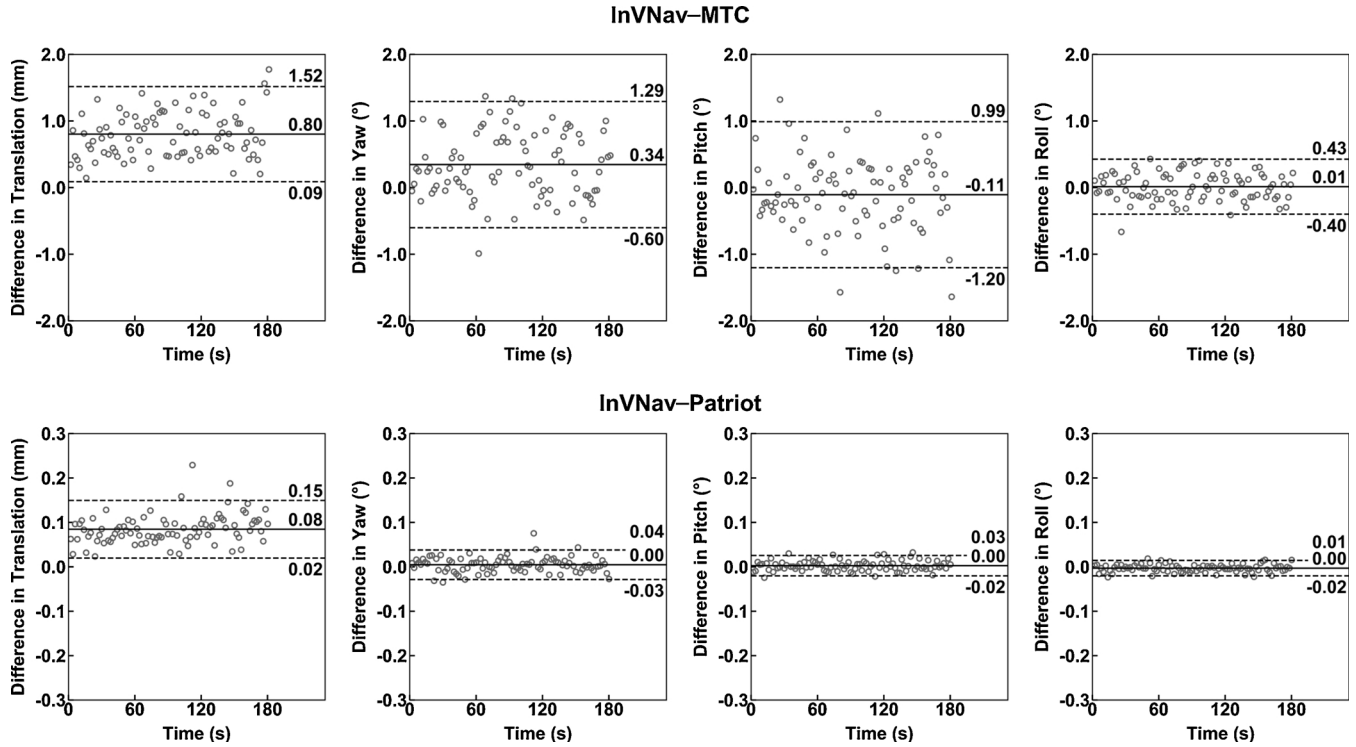

Fig. 6. Difference between measurements of translation and rotation angles (yaw, pitch, and roll) to target during navigation with InVesalius connected to MTC and Patriot (InVNav–MTC and InVNav–Patriot, respectively). Data points are the coordinates sampled every 2 s for 180 s, with coil and head static during the experiment to validate instrument position and orientation. The solid line represents the average and dashed lines represent 1.96 times the standard deviation (95% intervals) for each coordinate.

InVesalius Navigator stands out in comparison with commercially available navigation systems by being able to communicate with several spatial tracking devices, by its portability and minimum operational requirements. The software enables navigation and use of the target interface without an individual MRI by means of the MNI152 brain template (Fonov et al., 2011). InVesalius Navigator can be used with any TMS coil model, or any other instrument, and might be customizable to operate with recently developed controllable (Peterchev et al., 2014) and multi-locus TMS devices (Koponen et al., 2018). The software also provides methods for image and data manipulation such as segmentation and processing tools, and might be integrated straightforwardly to existing tools for neuroimaging analysis and TMS control such as MNE (Gramfort, 2013) and MagPy (McNair, 2017). InVesalius Navigator is distributed as an executable file that allows Windows (Microsoft Corporation) end users to install it easily [https://www.cti.gov.br/invesalius]. The source code with instructions for developers is hosted in a GitHub repository for version control [https://github.com/invesalius/invesalius3; (Souza et al., 2018)], and to allow third-party contributors to incorporate relevant features for their applications.

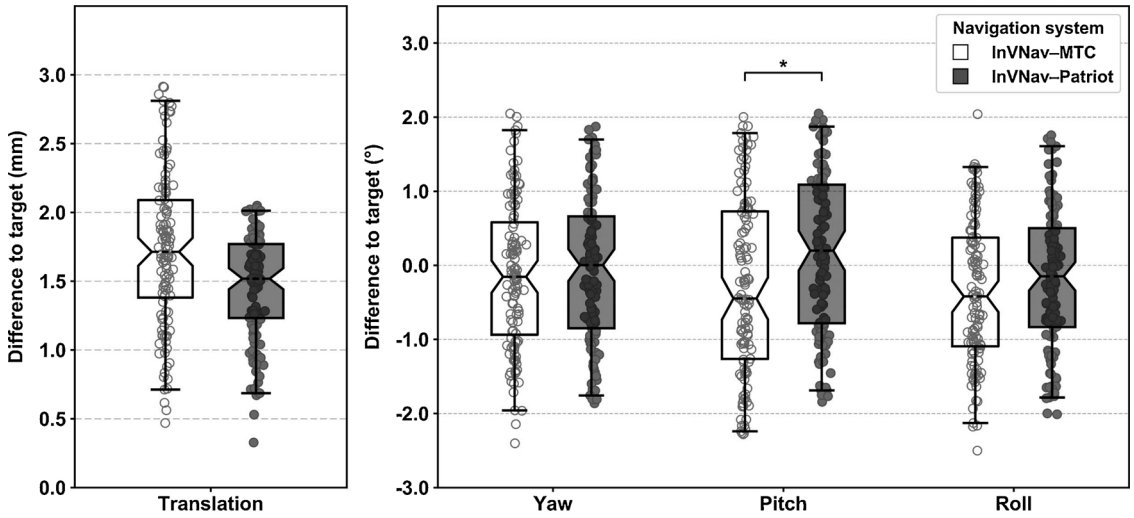

Fig. 7. The difference to the target in translation and rotation angles (yaw, pitch, and roll) in the target revisiting experiment for InVesalius connected to MTC (InVNav–MTC; white boxes) and Patriot (InVNav–Patriot; gray boxes). The box in the boxplot extends from the first to the third quartile of the data with the horizontal dashed line as the median, the notch represents the confidence interval around the median and the whiskers extend to the first data point equal to or 1.5 times less beyond the interquartile range. * p = 0.005.

5. Conclusion

Our study showed that InVesalius Navigator provides accurate neuronavigation within the acceptance range discussed in the literature. The errors obtained during navigation are comparable to those of other commercial systems. Finally, InVesalius Navigator is the first image-guided, open-source and free navigation software program for TMS coil positioning and might be used to improve the reliability of physiological experiments across different research and clinical centers.

Conflicts of interest

The authors declare no conflicts of interest.

Acknowledgements

This work was supported by the Fundação de Amparo à Pesquisa do Estado de São Paulo [FAPESP; grant numbers 2005/03293-2, 2009/09064-6 and 2012/11937-0], and by Conselho Nacional de Desenvolvimento Científico e Tecnológico [CNPq; grant number 140787/2014-3]. The study was partially funded by the Coordenação de Aperfeiçoamento de Pessoal de Nível Superior [CAPES; grant number DS447446]. Measurements with Nexstim NBS systems were performed at BioMag Laboratory, HUS Medical Imaging Center, University of Helsinki and Helsinki University Hospital, Finland. We thank Carlos Renato, Lourenço Rocha and Elcio Navas for technical support, and Iasmyn Oliveira for designing the virtual TMS coil model. We also thank Eduardo Rodrigues, Anderson Apunike, Vitor Cuziol and Tatiana Al-Chueyr for critical contributions to the software development.

Appendix A

Consider a coordinate system E that belongs to $\mathbb{R}^3$. The aim is to find the change of basis matrix from the canonical reference system $\mathbb{R}^3$ to E. To do so, we first need to collect three distinct points, P_1, P_2 and P_3 with coordinates given in $\mathbb{R}^3$. Then, a vector $\mathbf{v}_1^{aux}$ is created subtracting P_2 from P_1. A second vector $\mathbf{v}_2^{aux}$ is created subtracting P_3 from P_1. The point resulting from the projection of $\mathbf{v}_2^{aux}$ in $\mathbf{v}_1^{aux}$ will be used as the origin Q. Then, vector $\mathbf{v}_1$ is computed from P_3 to Q and $\mathbf{v}_2$ is computed from P_1 to Q. Vector $\mathbf{v}_3$ is obtained by the cross product between $\mathbf{v}_1$ and $\mathbf{v}_2$. Then, we define the correspondent transformation matrix of E.

$$\mathbf{v}_1 = \frac{P_1 - Q}{|P_1 - Q|} \tag{A1}$$

$$\mathbf{v}_2 = \frac{P_2 - Q}{|P_2 - Q|} \tag{A2}$$

$$\mathbf{v}_3 = \mathbf{v}_1 \times \mathbf{v}_2 \tag{A3}$$

$$M = \begin{bmatrix} v_{1,1} & v_{2,1} & v_{3,1} \\ v_{1,2} & v_{2,2} & v_{3,2} \\ v_{1,3} & v_{2,3} & v_{3,3} \end{bmatrix} \tag{A4}$$

References

Ambrosini, E., Ferrante, S., van de Ruit, M., Biguzzi, S., Colombo, V., Monticone, M., Ferriero, G., Pedrocchi, A., Ferrigno, G., Grey, M.J., 2018. StimTrack: an open-source software for manual transcranial magnetic stimulation coil positioning. J. Neurosci. Methods 293, 97–104. https://doi.org/10.1016/j.jneumeth.2017.09.012.

Amorim, P., Moraes, T., Silva, J., Pedrini, H., 2015. InVesalius: an interactive rendering framework for health care support. In: Bebis, G., Boyle, R., Parvin, B., Koracin, D., Pavlidis, I., Feris, R., McGraw, T., Elendt, M., Kopper, R., Ragan, E., Ye, Z., Weber, G. (Eds.), Advances in Visual Computing: 11th International Symposium, ISVC 2015. Las Vegas, NV, USA, December 14–16, 2015, Proceedings, Part I. Springer International Publishing, Cham, Switzerland. pp. 45–54. https://doi.org/10.1007/978-3-319-27857-5_5.

Chiarelli, A.M., Maclin, E.L., Low, Ka., Fabiani, M., Gratton, G., 2015. Comparison of procedures for co-registering scalp-recording locations to anatomical magnetic resonance images. J. Biomed. Opt. 20, 016009. https://doi.org/10.1117/1.JBO.20.1.016009.

Clarkson, M.J., Zombori, G., Thompson, S., Totz, J., Song, Y., Espak, M., Johnsen, S., Hawkes, D., Ourselin, S., 2015. The NifTK software platform for image-guided interventions: platform overview and NiftyLink messaging. Int. J. Comput. Assist. Radiol. Surg. 10, 301–316. https://doi.org/10.1007/s11548-014-1124-7.

Fedorov, A., Beichel, R., Kalpathy-Cramer, J., Finet, J., Fillion-Robin, J.-C., Pujol, S., Bauer, C., Jennings, D., Fennessy, F., Sonka, M., Buatti, J., Aylward, S., Miller, J.V., Pieper, S., Kikinis, R., 2012. 3D Slicer as an image computing platform for the Quantitative Imaging Network. Magn. Reson. Imaging 30, 1323–1341. https://doi.org/10.1016/j.mri.2012.05.001.

Fitzpatrick, J.M., West, J.B., Maurer, C.R., 1998. Predicting error in rigid-body point-based registration. IEEE Trans. Med. Imaging 17, 694–702. https://doi.org/10.1109/42.736021.

Fonov, V., Evans, A.C., Botteron, K., Almli, C.R., McKinstry, R.C., Collins, D.L., 2011. Unbiased average age-appropriate atlases for pediatric studies. Neuroimage 54, 313–327. https://doi.org/10.1016/j.neuroimage.2010.07.033.

Gramfort, A., 2013. MEG and EEG data analysis with MNE-Python. Front. Neurosci. 7. https://doi.org/10.3389/fnins.2013.00267.

Grillo, F.W., Souza, V.H., Matsuda, R.H., Rondinoni, C., Pavan, T.Z., Baffa, O., Machado, H.R., Carneiro, A.A.O., 2018. Patient-specific neurosurgical phantom: assessment of visual quality, accuracy, and scaling effects. 3D Print. Med. 4, 3. https://doi.org/10.1186/s41205-018-0025-8.

Horn, B.K.P., 1987. Closed-form solution of absolute orientation using unit quaternions. J. Opt. Soc. Am. A 4, 629. https://doi.org/10.1364/JOSAA.4.000629.

Julkunen, P., 2014. Methods for estimating cortical motor representation size and location in navigated transcranial magnetic stimulation. J. Neurosci. Methods 232, 125–133. https://doi.org/10.1016/j.jneumeth.2014.05.020.

Koponen, L.M., Nieminen, J.O., Ilmoniemi, R.J., 2018. Multi-locus transcranial magnetic stimulation—theory and implementation. Brain Stimul. https://doi.org/10.1016/j.brs.2018.03.014.

Kuehn, B., Mularski, S., Schoenherr, S., Hammersen, S., Stendel, R., Kombos, T., Suess, S., Suess, O., 2008. Sensor-based neuronavigation: evaluation of a large continuous patient population. Clin. Neurol. Neurosurg. 110, 1012–1019. https://doi.org/10.1016/j.clineuro.2008.06.017.

Laakso, I., Murakami, T., Hirata, A., Ugawa, Y., 2018. Where and what TMS activates: experiments and modeling. Brain Stimul. 11, 166–174. https://doi.org/10.1016/j.brs.2017.09.011.

Little, G., Boe, S., Bardouille, T., 2014. Head movement compensation in real-time magnetoencephalographic recordings. MethodsX 1, 275–282. https://doi.org/10.1016/j.mex.2014.10.008.

Maciunas, R.J., Galloway Jr., R.L., Latimer, J., Cobb, C., Zaccharias, E., Moore, A., Mandava, V.R., 1992. An independent application accuracy evaluation of stereotactic frame systems. Stereotact. Funct. Neurosurg. 58, 103–107. https://doi.org/10.1159/000098981.

Mascott, C.R., 2006. In vivo accuracy of image guidance performed using optical tracking and optimized registration. J. Neurosurg. 105, 561–567. https://doi.org/10.3171/jns.2006.105.4.561.

McNair, N.A., 2017. MagPy: a Python toolbox for controlling Magstim transcranial magnetic stimulators. J. Neurosci. Methods 276, 33–37. https://doi.org/10.1016/j.jneumeth.2016.11.006.

Nolden, M., Zelzer, S., Seitel, A., Wald, D., Müller, M., Franz, A.M., Maleike, D., Fangerau, M., Baumhauer, M., Maier-Hein, L., Maier-Hein, K.H., Meinzer, H.-P., Wolf, I., 2013. The medical imaging interaction Toolkit: challenges and advances. Int. J. Comput. Assist. Radiol. Surg. 8, 607–620. https://doi.org/10.1007/s11548-013-0840-8.

Omara, A.I., Wang, M., Fan, Y., Song, Z., 2014. Anatomical landmarks for point-matching registration in image-guided neurosurgery. Int. J. Med. Robot. Comput. Assist. Surg. 10, 55–64. https://doi.org/10.1002/rcs.1509.

Orringer, D., Golby, A., Jolesz, F., 2012. Neuronavigation in the surgical management of brain tumors: current and future trends. Expert Rev. Med. Devices 9, 491–500. https://doi.org/10.1586/erd.12.42.

Peirce, J.W., 2007. PsychoPy—psychophysics software in Python. J. Neurosci. Methods 162, 8–13. https://doi.org/10.1016/j.jneumeth.2006.11.017.

Peres, A.S.C., Souza, V.H.O., Maziero, D., de Araujo, D.B., Salmon, C.E.G., Baffa, O., 2009. Vector magnetic field mapping of a transcranial magnetic stimulation coil using magnetic resonance imaging: in vitro and in vivo experiments. IFMBE Proceedings, World Congress on Medical Physics and Biomedical Engineering: Diagnostic and Therapeutic Instrumentation, Clinical Engineering 571–574. https://doi.org/10.1007/978-3-642-03885-3_159.

Peterchev, A.V., D'Ostilio, K., Rothwell, J.C., Murphy, D.L., 2014. Controllable pulse parameter transcranial magnetic stimulator with enhanced circuit topology and pulse shaping. J. Neural Eng. 11, 056023. https://doi.org/10.1088/1741-2560/11/5/056023.

Poggi, S., Pallotta, S., Russo, S., Gallina, P., Torresin, A., Bucciolini, M., 2003. Neuronavigation accuracy dependence on CT and MR imaging parameters: a phantom-based study. Phys. Med. Biol. 48, 2199–2216. https://doi.org/10.1088/0031-9155/48/14/311.

Rondinoni, C., Souza, V.H.O., Matsuda, R.H., Salles, A.C.P., Santos, M.V., Filho, O.B., dos Santos, A.C., Machado, H.R., Noritomi, P.Y., da Silva, J.V.L., 2014. Inter-institutional protocol describing the use of three-dimensional printing for surgical planning in a patient with childhood epilepsy: from 3D modeling to neuronavigation. 2014 IEEE 16th International Conference on E-Health Networking, Applications and Services (Healthcom) 347–349. https://doi.org/10.1109/HealthCom.2014.7001866.

Rossini, P.M., Burke, D., Chen, R., Cohen, L.G., Daskalakis, Z., Di Iorio, R., Di Lazzaro, V., Ferreri, F., Fitzgerald, P.B., George, M.S., Hallett, M., Lefaucheur, J.P., Langguth, B., Matsumoto, H., Miniussi, C., Nitsche, M.A., Pascual-Leone, A., Paulus, W., Rossi, S., Rothwell, J.C., Siebner, H.R., Ugawa, Y., Walsh, V., Ziemann, U., 2015. Non-invasive electrical and magnetic stimulation of the brain, spinal cord, roots and peripheral nerves: basic principles and procedures for routine clinical and research application. An updated report from an I.F.C.N. Committee. Clin. Neurophysiol. 126, 1071–1107. https://doi.org/10.1016/j.clinph.2015.02.001.

Ruohonen, J., Karhu, J., 2010. Navigated transcranial magnetic stimulation. Neurophysiol. Clin. 40, 7–17. https://doi.org/10.1016/j.neucli.2010.01.006.

Sollmann, N., Goblirsch-Kolb, M.F., Ille, S., Butenschoen, V.M., Boeckh-Behrens, T., Meyer, B., Ringel, F., Krieg, S.M., 2016. Comparison between electric-field-navigated and line-navigated TMS for cortical motor mapping in patients with brain tumors. Acta Neurochir. 158, 2277–2289. https://doi.org/10.1007/s00701-016-2970-6.

Souza, V.H., Vieira, T.M., Peres, A.S.C., Garcia, M.A.C., Vargas, C.D., Baffa, O., 2017. Effect of TMS coil orientation on the spatial distribution of motor evoked potentials in an intrinsic hand muscle. Biomed. Eng./Biomed. Tech. https://doi.org/10.1515/bmt-2016-0240. Ahead of print.

Souza, V.H., Matsuda, R.H., Peres, A.S.C., Amorim, P.H.J., Moraes, T.F., Silva, J.V.L., Baffa, O., 2018. Vesalius Navigator: Neuronavigation Software. https://doi.org/10.5281/ZENODO.1326396.

Steinmeier, R., Rachinger, J., Kaus, M., Ganslandt, O., Huk, W., Fahlbusch, R., 2000. Factors influencing the application accuracy of neuronavigation systems. Stereotact. Funct. Neurosurg. 75, 188–202. https://doi.org/10.1159/000048404.

Tsuzuki, D., Dan, I., 2014. Spatial registration for functional near-infrared spectroscopy: from channel position on the scalp to cortical location in individual and group analyses. Neuroimage 85 (Pt 1), 92–103. https://doi.org/10.1016/j.neuroimage.2013.07.025.